

# Petrographic and Geochemical Characteristics of the Akaba Igneous Massif from the Pan-African Orogen in Togo, West Africa

Sarakawa Abalo Malibida KPANZOU<sup>1,2\*</sup> Gnanwasou ALAYI<sup>1</sup> Essodina PADARO<sup>1</sup>  
Mahaman Sani TAIROU<sup>1</sup> Yao AGBOSOUMONDE<sup>1</sup>

1. Department of Geology, Faculty of Sciences, University of Lomé, 01 P.O Box 1515 Lomé 1, Lomé, Togo  
2. Department of Civil Engineering, Laboratory of Geotechnics and Mining, Regional Training Center for Road Maintenance (CERFER - Entente Council), P.O Box 1369 Lomé, Lomé, Togo

\*Corresponding author: germalibida@gmail.com

## Abstract

The Dahomeyide orogen in Togo and adjoining parts of southeast-Ghana and Benin represents the West Africa Craton (WAC) suture into northwest Gondwana. The suture zone is a narrow and lithologically diverse region with high pressure granulites complexes. The Akaba massif located in the central part of Togo, belongs to this suture zone. Petrographical and whole rock geochemical analyses are used to evaluate the characteristics, petrogenesis and mode of emplacement of the Akaba massif. The new data suggest that the Akaba massif is built by layered amphibolites, garnet-free granulites and metapyroxenites. These rocks were equilibrated under granulite facies conditions and subsequently partially retrogressed to the amphibolite facies. Geochemical suggest that the granulites may have preserved the geochemical imprints of their igneous protoliths. They display tholeiitic affinity, slightly enriched LREE, no Eu anomaly and negative anomalies in Nb and Zr indicate subduction zone magmatism. These features are consistent with protoliths of N-MORB affinities. The Akaba massif rocks were emplaced up in an oceanic arc environment and likely originated from a metasomatized mantle.

**Keywords:** Granulites, Petrography, Geochemistry, Akaba massif, Pan-African orogen, West Africa.

**DOI:** 10.7176/JEES/13-7-03

**Publication date:** September 30<sup>th</sup> 2023

## 1. Introduction

In the Pan-African Dahomeyide belt, the basic to ultrabasic complexes of Derouvarou (Benin), Kabye-Kpaza, Djabatoure-Anie, Agou-Ahito (Togo), and Shaï or Akuse (Ghana) from a submeridian mountainous belt materializing the suture zone (Ménot & Séddoh, 1980; Agbossoumondé, 1998; Attoh, 1998; Agbossoumondé *et al.*, 2001; Tairou & Affaton, 2013). The Akaba massif in central Togo represents one of the elements of this belt. It is defined, like the other massifs of this suture zone, as a highly metamorphic ophiolitic-type unit. It is composed of ultramafic, gabbroic metacumulates, metagabbros, metadolerites, metabasalts, pyroxenites, amphibolites and granulites (Ménot, 1977, 1980, 1982; Ménot & Séddoh, 1980; Agbossoumondé, 1998; Duclaux, 2003; Agbossoumondé *et al.*, 2007; Kpanzou, 2017, 2023; Kpanzou *et al.*, 2019, 2022, 2023). Previous studies (Duclaux, 2003; Sabi, 2007; Agbossoumondé *et al.*, 2007) have partially addressed the petrographic and geochemical characteristics of all the massifs in the togoese segment of the suture zone. According to these studies, the Akaba massif is composed of pyroxenites and gabbros. It shows a signature of continental tholeiite emplaced in the continental crust and slow cooling during exhumation. It is also believed that the rocks of the Akaba massif underwent metamorphism in the granulite facies with a retrogression in the amphibolite facies associated with the nappes emplacement. These are meta- to peraluminous rocks with a tholeiitic signature, emplaced in a continental arc context and exhumed during the Pan-African tangential phase.

Despite efforts to better understand the petrography and geochemistry of Akaba massif rocks, detailed petrographic and geochemical characterization of the rocks of this massif remains are lacking. Therefore, the present study is a contribution to the detailed petrographic and geochemical study of the rocks of the Akaba massif. Specifically, the aims to provide (i) a detailed petrographic description of the Akaba massif rocks, (ii) a rock classification and origin, (iii) and geodynamic environment.

## 2. Geological context

The Pan-African Dahomeyide belt resulted from the collision between 3 structures: the eastern portion of the WAC, the Benino-Nigerian basement and the Touareg Shield (Caby *et al.*, 1981; Attoh *et al.*, 1997; Ganade de Araujo *et al.*, 2014a). It is subdivided into three structural zones which are from west to east: the external zone, the suture zone and the internal zone (Affaton, 1990) (Figure 1).

The external zone corresponds to the Buem and Atacora structural units. The Buem is composed of metasedimentary rocks that originated from the metamorphism of the Volta Basin units. The Atacora consists of orthogneissic units of Kara-Niamtougou and the granitoids of the Kpalimé-Amlamé pluton (Affaton, 1990;

Affaton *et al.*, 1991; Agbossoumondé *et al.*, 2007; Tairou *et al.*, 2009; Aidoo *et al.*, 2020; Kwayisi *et al.*, 2021; Tairou *et al.*, 2022). The external zone overlaps the WAC and its sedimentary cover.

The suture zone is materialized by a submeridian alignment of complexes: Derouvarou in Benin, Kabye-Kpaza, Djabatoure-Anie and Agou-Ahito in Togo, and Akuse or Shaï in Ghana. These complexes are composed of mafic to ultramafic rocks (granulite or sometimes eclogite facies), evidence of Pan-African crustal thickening (Ménot & Séddoh, 1985; Attoh, 1998; Agbossoumondé *et al.*, 2001; Attoh & Morgan, 2004; Aidoo *et al.*, 2020; Kpanzou, 2023).

The internal zone is a peneplain representing the remobilized Benino-Nigerian shield (BNS) in the Pan-African belt (Affaton, 1990). It is composed of gneisso-migmatitic, metasedimentary (schists, marbles and quartzites) and Pan-African granitoids units (Affaton *et al.*, 1991; Caby & Boessé, 2001; Alayi, 2018).

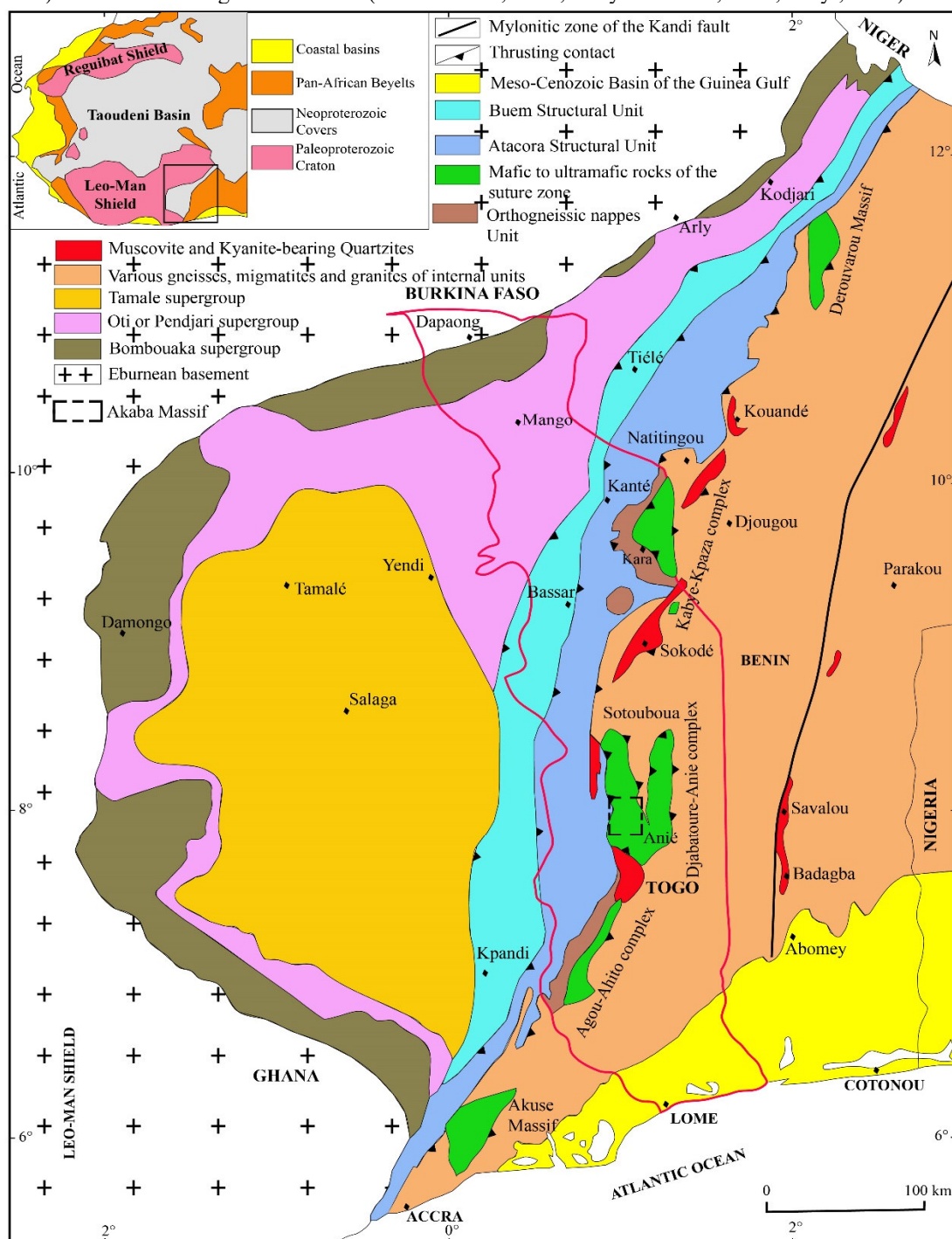


Figure 1. Simplified geologic map showing the main structural domains of the Pan-African Dahomeyide belt and its foreland (Affaton, 1990; slightly modified) with the location of the Akaba massif.

### 3. Methodology

This study is based on a literature review of previous work, field work, laboratory analysis, data processing and analysis. The literature review allowed for a synthesis of previous work on regional geology and the geology of the study area. The field campaign allowed us to search for outcrops and collect samples, as well as to describe these outcrops and samples macroscopically in situ. We georeferenced the outcrops and sampling stations using a Garmin eTrex Legend H GPS. Several rock samples were selected during the field campaign. Fifteen (15) thin sections of these rocks were prepared at the Center for Geological and Mining Research (CRGM) at Niamey (Republic of Niger). These thin sections were studied under an OPTIKA petrographic microscope at the University of Lomé (Togo) to identify the main minerals and the nature of the rocks. Nine (09) carefully selected rock samples were sent to the Center for Scientific Instrumentation of the University of Granada (CIC-UGR) in Spain for geochemical analysis.

The analytical approach adopted is as follows:

- (i) Major elements oxides were determined with a Philips Magix Pro (Pw-2440) X-ray fluorescence (XRF) equipment after melting the rock sample in a solution with tetra lithium borate. The characteristic precision as determined from standards AN-G and BEN, was better than  $\pm 1.5\%$  (relative error) for an analyte concentration of 10 wt.%. The iron content is expressed as FeO\* total. The molar ratio MgO/(MgO+FeO\*) is abbreviated Mg#. Zirconium was determined with the same instrument using the same glass beads with a precision better than  $\pm 0.2\%$  for 5 ppm Zr. Loss on Ignition (LOI) was determined by weight difference before and after ignition of samples in a furnace. In the diagrams, oxide concentrations are reported in an anhydrous (volatile free) basis.
- (ii) Trace elements, except Zr, were determined by an Inductively Coupled Plasma-Mass Spectrometry (ICP-MS) after  $\text{HNO}_3 + \text{HF}$  digestion of 0.1000 g of sample powder in a Teflon-lined vessel at  $180^\circ\text{C}$  and 200 psi for 30 min, evaporation to dryness and subsequent dissolution in 100 ml of 4 vol.%  $\text{HNO}_3$ ; the precision, as determined from standards PMS, WSE, UBN, BEN, BR and AGV run as unknowns, was better than  $\pm 2\%$  for analyte concentrations of 50 ppm and  $\pm 5\%$  for analyte concentrations of 5 ppm.

The results of the chemical analyses are reported in table 1. The location of the analyzed samples is shown in Figure 2. Field and chemical analysis data were compiled in Excel and imported into various software packages (GCDkit, QGIS, etc.) for specific processing. For geochemical data processing, we proceeded to the normalization of major elements to 100% under anhydrous basis.

## 4. Results

### 4.1 Petrography

The Akaba massif (Figure 2) is essentially composed of metapyroxenites, granulites and amphibolites.

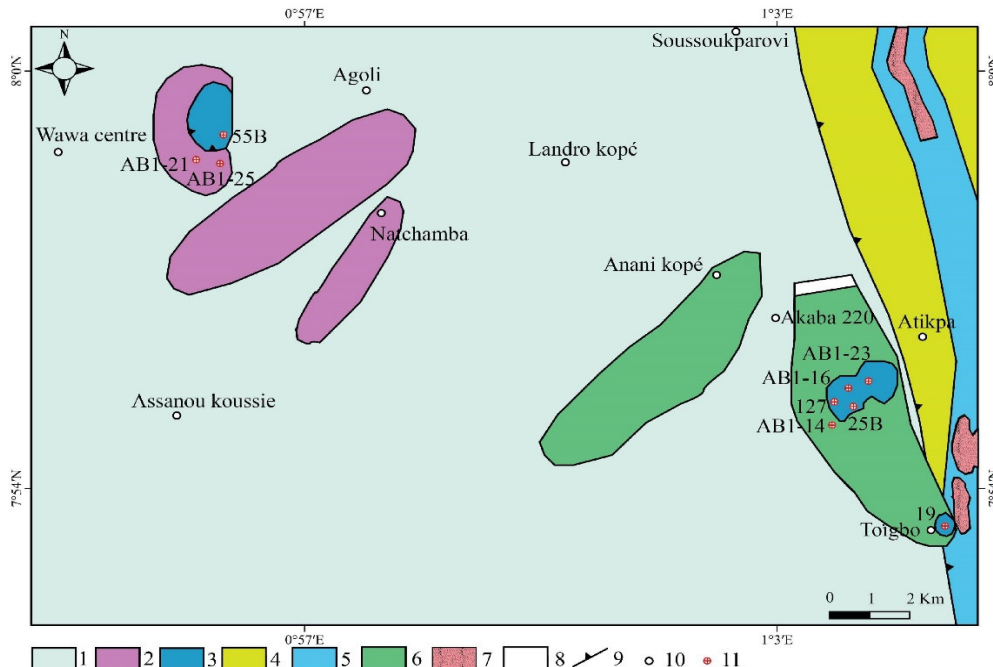


Figure 2. Schematic map of the Akaba massif showing the location of the samples analyzed (modified from the geological map of Sylvain *et al.*, 1986).

1: biotite- and amphibole-bearing gneiss; 2: granulites; 3: metapyroxenites; 4: 2-mica-bearing paragneiss; 5: biotite-bearing micaschists; 6: amphibolites; 7: biotite-bearing quartzites; 8: quartz veins; 9: overlapping contact; 10: towns and villages; 11: samples.

#### 4.1.1 Metapyroxenites

Metapyroxenites outcrop in very dense dark gray to black balls (Figure 3a). They are massive and mainly composed of pyroxene of variable size, to which amphiboles and rarely plagioclases are added. Microscopically, they have a granoblastic (cumulative) texture (Figure 3b) composed of pyroxene, amphibole, plagioclase and opaque minerals. Clinopyroxene (diopside) is globular and very abundant. It shows undulating extinction, epidote retromorphoses and numerous inclusions of amphibole and oxides (ilmenite, magnetite). Reddish-brown orthopyroxene (hypersthene) is globular and contiguous with clinopyroxene. It shows cleavage and undulate extinction. Plagioclase in subautomorphic phenocrysts displays polysynthetic twin and sometimes small xenomorphic interstitial patches. Acicular amphibole is of the brown hornblende type. It occurs as elongated phenocrysts, sometimes containing inclusions of oxides (ilmenite, magnetite), or as small interstitial crystals or inclusions in clinopyroxenes.

#### 4.1.2 Granulites

They outcrop in mylonitized benches at the base of the Agoli metapyroxenites (Figure 3c) or in balls within the Akaba 220 metapyroxenites. They are grayish, foliated or sometimes massive and fine to medium-grained. Microscopically, they have a granoblastic texture (Figure 3d). Their mineralogy consists of plagioclase, clinopyroxene, amphibole and oxides. Plagioclase is abundant, often in the form of subautomorphic crystals with polysynthetic twin. Clinopyroxene (diopside) occurs as blasts and is intensely cracked. Amphiboles (green hornblende) show cleavages lined with oxides and epidote.

#### 4.1.3 Amphibolites

They outcrop in centimetric to metric benches at the contact with granulites and metapyroxenites at Akaba 220 (Figure 3e). They cut into dark-gray, foliated, fine-grained platelets. Microscopic examination reveals a nematogranoblastic texture (Figure 3f) composed of amphibole, plagioclase, quartz and oxides. Amphibole (brown hornblende) in elongated (acicular) crystals is abundant and highlights the ferromagnesian beds. Plagioclases are xenomorphic, form the clear beds and present sections associated with the rare quartz minerals. Quartz, with its undulate extinction, is not very abundant and is in association with plagioclase in the clear beds.

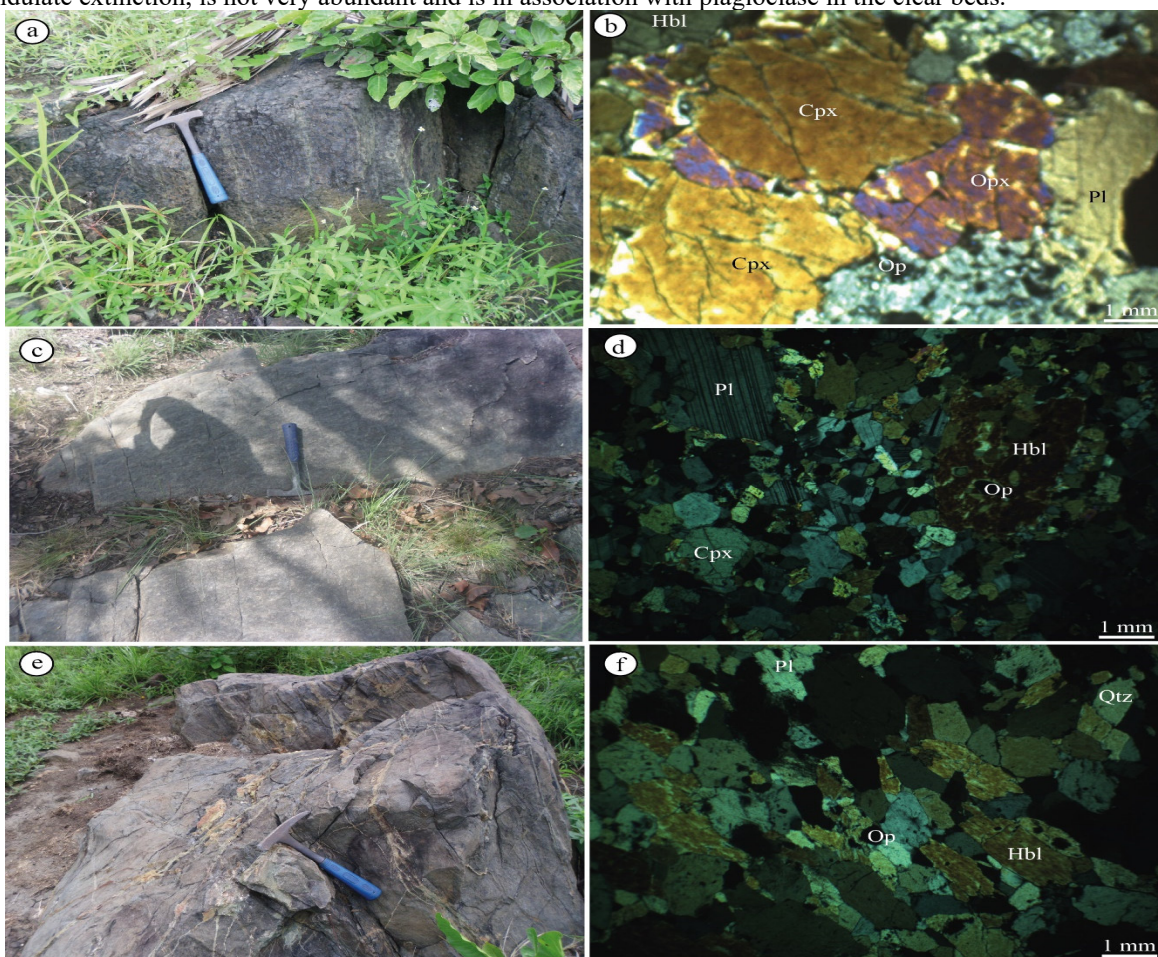


Figure 3. Macroscopic (a, c and e) and microscopic (b, d and f) photography of the Akaba massif rocks. (a and b): metapyroxenite; (c and d): granulite; (e and f): amphibolite. Opx: orthopyroxene; Cpx: clinopyroxene; Pl: plagioclase; Hbl: hornblende; Qtz: quartz; Op: opaque.

## 4.2 Geochemistry

### 4.2.1 Major elements distribution

The Akaba massif rocks are characterized by silica contents in the range of 44.59% to 52.29% (Table 1). They are mainly granulites, metapyroxenites and amphibolites. The analyzed samples show values high of Al<sub>2</sub>O<sub>3</sub> up to 16.48% and Sr up to 235.6 ppm which implies their richness in plagioclase. MgO contents reach 22.49% and Fe<sub>2</sub>O<sub>3</sub> up to 15.11%, indicating pyroxene accumulation.

According to Harker diagram (Figure 4), Akaba massif rocks show a positive correlation between SiO<sub>2</sub> and MgO, and negative with TiO<sub>2</sub>, Al<sub>2</sub>O<sub>3</sub>, Na<sub>2</sub>O, K<sub>2</sub>O and P<sub>2</sub>O<sub>5</sub>. The increase in MgO reflects the crystallization of pyroxene and amphibole. The decrease in TiO<sub>2</sub> and P<sub>2</sub>O<sub>5</sub> indicates fractional crystallization of ilmenite and apatite. The decrease in Al<sub>2</sub>O<sub>3</sub>, Na<sub>2</sub>O and K<sub>2</sub>O reflects the alkali feldspar content of these rocks.

Table 1. Results of geochemical analyses of major elements (%), traces elements (ppm) and rare earth elements (ppm) of the Akaba massif rocks.

| Lithology                      | Granulites   |               |              | Metapyroxenites |              |              |              | Amphibolites |              |
|--------------------------------|--------------|---------------|--------------|-----------------|--------------|--------------|--------------|--------------|--------------|
| Ech.                           | AB 1-21      | AB 1-25       | 19           | 25B             | 55B          | 127          | AB 1-16      | AB 1-23      | AB 1-14      |
| Xcoord.                        | E0°55'27,7"  | E0°55'27,7"   | E1°05'15,6"  | E1°04'07,1"     | E0°55'31,9"  | E1°04'19,9"  | E1°03'41,9"  | E1°03'41,9"  | E1°03'19,0"  |
| Ycoord.                        | N7°58'28,4"  | N7°58'28,4"   | N7°53'31,1"  | N7°55'09,3"     | N7°59'01,7"  | N7°55'26,5"  | N7°55'03,3"  | N7°55'03,3"  | N7°55'01,4"  |
| <b>Majors (%)</b>              |              |               |              |                 |              |              |              |              |              |
| SiO <sub>2</sub>               | 48,36        | 48,6          | 50,57        | 44,59           | 50,40        | 52,28        | 52,29        | 50,33        | 45,2         |
| Al <sub>2</sub> O <sub>3</sub> | 7,02         | 12,38         | 13,53        | 11,61           | 5,92         | 4,57         | 2,8          | 5,64         | 16,48        |
| Fe <sub>2</sub> O <sub>3</sub> | 11,65        | 9,86          | 12,59        | 11,23           | 9,80         | 10,12        | 11,22        | 11,19        | 15,11        |
| MnO                            | 0,23         | 0,14          | 0,19         | 0,15            | 0,18         | 0,21         | 0,23         | 0,22         | 0,2          |
| MgO                            | 15,25        | 13,13         | 7,28         | 13,39           | 16,62        | 15,35        | 22,49        | 17,27        | 6,45         |
| CaO                            | 14,16        | 12,08         | 11,27        | 12,35           | 15,16        | 14,01        | 8,58         | 12,31        | 10,86        |
| Na <sub>2</sub> O              | 1,38         | 2,43          | 2,12         | 1,59            | 0,72         | 0,89         | 0,28         | 0,94         | 2,58         |
| K <sub>2</sub> O               | 0,51         | 0,42          | 0,22         | 0,54            | 0,06         | 0,19         | 0,07         | 0,19         | 0,13         |
| TiO <sub>2</sub>               | 1,17         | 1,15          | 1,21         | 2,45            | 0,83         | 0,66         | 0,38         | 0,96         | 1,85         |
| P <sub>2</sub> O <sub>5</sub>  | 0,04         | 0,12          | 0,10         | 0,06            | 0,02         | 0,04         | 0,01         | 0,06         | 0,16         |
| PAF                            | 0,83         | 0,94          | 0,35         | 1,45            | 0,00         | 1,18         | 0,83         | 0,52         | -            |
| Total                          | <b>100,6</b> | <b>101,24</b> | <b>99,43</b> | <b>99,41</b>    | <b>99,71</b> | <b>99,50</b> | <b>99,18</b> | <b>99,63</b> | <b>99,01</b> |
| <b>Traces (ppm)</b>            |              |               |              |                 |              |              |              |              |              |
| Rb                             | <2,0         | <2,0          | 8,11         | 5,35            | 0,54         | 1,49         | <2,0         | <2,0         | <2,0         |
| Ba                             | 94           | 82,2          | 106,94       | 153,09          | 33,64        | 17,98        | 38,1         | 148,8        | 70,1         |
| Nb                             | 3,7          | 3             | 3,73         | 3,48            | 1,25         | 1,22         | 4,00         | 3,3          | 3,3          |
| Ta                             | -            | -             | 0,33         | 0,21            | 0,10         | 0,06         | -            | -            | -            |
| Sr                             | 108,8        | 224,2         | 112,24       | 196,69          | 68,52        | 35,70        | 15,1         | 52,7         | 235,6        |
| Zr                             | 50,5         | 43,9          | 57,70        | 49,00           | 30,10        | 38,60        | 34,4         | 67,6         | 50,3         |
| Y                              | 21,3         | 14,6          | 23,58        | 28,74           | 17,90        | 22,00        | 20           | 28,8         | 19,5         |
| Hf                             | <3,0         | <3,0          | 0,39         | 1,48            | 1,01         | 0,47         | 4,4          | <3,0         | <3,0         |
| Ni                             | 217,8        | 270,8         | 123,97       | 237,46          | 368,78       | 473,41       | 412,2        | 317,7        | 95,1         |
| Cr                             | -            | -             | 229,47       | 478,28          | 649,82       | 969,40       | -            | -            | -            |
| V                              | -            | -             | 340,71       | 489,95          | 304,84       | 217,05       | -            | -            | -            |
| U                              | -            | -             | 0,11         | 0,08            | 0,01         | 0,14         | -            | -            | -            |
| Th                             | <3,0         | <3,0          | 0,00         | 0,00            | 0,00         | <3,0         | <3,0         | <3,0         | <3,0         |
| Sc                             | -            | -             | 41,30        | 63,31           | 64,79        | 48,36        | -            | -            | -            |
| Co                             | -            | -             | 70,89        | 68,75           | 72,42        | 71,68        | -            | -            | -            |
| Cu                             | -            | -             | 124,06       | 26,73           | 39,32        | 134,48       | -            | -            | -            |
| Zn                             | -            | -             | 77,90        | 75,54           | 53,60        | 78,73        | -            | -            | -            |
| Mo                             | -            | -             | 4,21         | 1,48            | 3,03         | 2,16         | -            | -            | -            |
| Cs                             | 8,9          | 11,1          | 0,20         | 0,22            | 0,07         | 0,08         | 8,7          | 7,7          | 9,1          |
| Li                             | -            | -             | 3,60         | 9,02            | 3,40         | 3,79         | -            | -            | -            |
| Be                             | -            | -             | 0,45         | 0,53            | 0,30         | 0,42         | -            | -            | -            |
| Ga                             | 11,2         | 15,5          | 16,96        | 15,14           | 9,54         | 8,33         | 7,7          | 10           | 18,2         |
| Sn                             | -            | -             | 0,50         | 1,06            | 0,43         | 0,37         | -            | -            | -            |
| Tl                             | -            | -             | 0,06         | 0,04            | 0,02         | 0,03         | -            | -            | -            |
| Pb                             | -            | -             | 2,45         | 3,31            | 0,14         | 1,03         | -            | -            | -            |
| <b>REE (ppm)</b>               |              |               |              |                 |              |              |              |              |              |
| La                             | <7,5         | <7,5          | 7,71         | 4,19            | 4,08         | 4,31         | 8,8          | 9,5          | <7,5         |
| Ce                             | 31,5         | 32,8          | 17,15        | 13,79           | 10,53        | 12,13        | 38,3         | 35,6         | 25,8         |
| Pr                             | -            | -             | 2,34         | 2,54            | 1,59         | 1,93         | -            | -            | -            |
| Nd                             | -            | -             | 11,09        | 14,43           | 7,84         | 10,45        | -            | -            | -            |
| Sm                             | -            | -             | 3,12         | 4,78            | 2,72         | 3,30         | -            | -            | -            |
| Eu                             | -            | -             | 1,15         | 1,73            | 0,83         | 1,17         | -            | -            | -            |
| Gd                             | -            | -             | 3,58         | 5,04            | 2,37         | 3,27         | -            | -            | -            |
| Tb                             | -            | -             | 0,52         | 0,76            | 0,44         | 0,53         | -            | -            | -            |
| Dy                             | -            | -             | 3,44         | 4,58            | 2,80         | 3,37         | -            | -            | -            |
| Ho                             | -            | -             | 0,77         | 0,94            | 0,60         | 0,72         | -            | -            | -            |
| Er                             | -            | -             | 1,96         | 2,24            | 1,52         | 1,84         | -            | -            | -            |
| Tm                             | -            | -             | 0,29         | 0,31            | 0,22         | 0,27         | -            | -            | -            |
| Yb                             | -            | -             | 1,74         | 1,78            | 1,27         | 1,61         | -            | -            | -            |
| Lu                             | -            | -             | 0,27         | 0,26            | 0,18         | 0,23         | -            | -            | -            |
| Eu/Eu*                         | -            | -             | 1,03         | 1,06            | 0,98         | 1,07         | -            | -            | -            |
| (La)N                          | -            | -             | 20,08        | 10,91           | 10,63        | 11,22        | -            | -            | -            |
| (Sm)N                          | -            | -             | 13,47        | 20,64           | 11,74        | 14,25        | -            | -            | -            |
| (Gd)N                          | -            | -             | 11,68        | 16,44           | 7,73         | 10,67        | -            | -            | -            |
| (Yb)N                          | -            | -             | 7,57         | 7,74            | 5,52         | 7,00         | -            | -            | -            |
| (La/Sm)N                       | -            | -             | 1,49         | 0,53            | 0,90         | 0,79         | -            | -            | -            |
| (Gd/Yb)N                       | -            | -             | 1,54         | 2,12            | 1,40         | 1,52         | -            | -            | -            |
| (La/Yb)N                       | -            | -             | 2,65         | 1,41            | 1,92         | 1,60         | -            | -            | -            |
| <b>ΣREE</b>                    | -            | -             | 55,13        | 57,37           | 36,99        | 45,13        | -            | -            | -            |

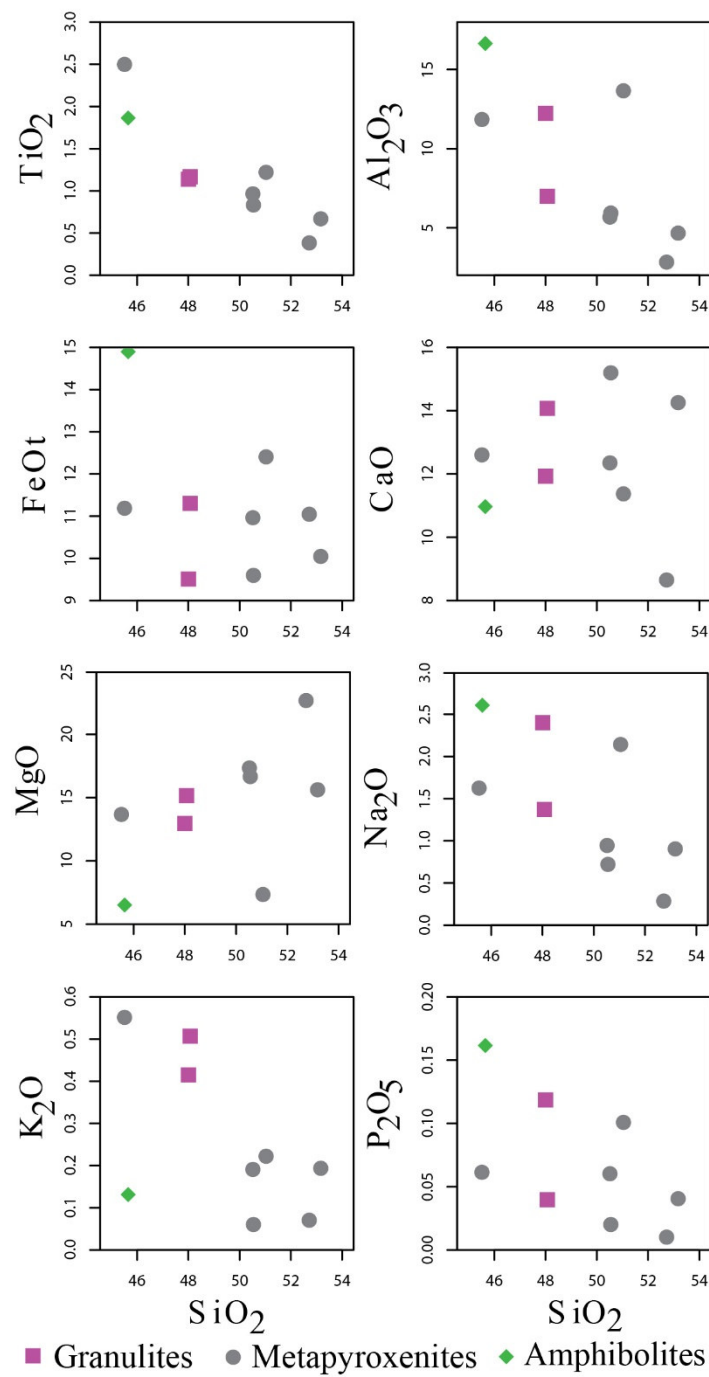


Figure 4. Oxides ( $\text{TiO}_2$ ,  $\text{FeOt}$ ,  $\text{Na}_2\text{O}$ ,  $\text{K}_2\text{O}$ ,  $\text{P}_2\text{O}_5$ ,  $\text{Al}_2\text{O}_3$ ,  $\text{CaO}$ ,  $\text{MgO}$ ) vs  $\text{SiO}_2$  variation diagrams in Akaba massif rocks (Harker, 1909).

#### 4.2.2 Traces and rare earth elements distribution

In the trace elements (Rb, Sr, Nd, Ba, Nb, Y, Ni, Cr) versus Zr diagrams (Harker, 1909) (Figure 5): rocks from the Akaba massif show a positive correlation between Zr and Rb, Ba, Nb, Nd, Y, La and negative with Sr and Ni. The Y fractionation of these rocks is associated with zircon, while the Rb and Ba fractionation with biotite. The negative correlation of Zr with Ni is compatible with fractionation of the ferromagnesians (pyroxene, amphibole) in these rocks.

Rare earth spectra normalized to chondrites (Nakamura, 1974) (Figure 6a) show that the rocks of the Akaba massif are weakly fractionated in light rare earth elements ( $0.53 \leq (\text{La}/\text{Sm})\text{N} \leq 1.49$ ) and show almost flat spectra in heavy rare earth elements ( $1.40 \leq (\text{Gd}/\text{Yb})\text{N} \leq 2.12$ ). This fractionation is indicated by  $(\text{La}/\text{Yb})\text{N}$  ratio between 1.41 and 2.65. They show slight positive anomalies in Pr, Ho, Tm and negative in Ce, Nd, Dy, Er, Yb.

Multi-element spectra normalized to the primitive mantle (McDonough & Sun, 1995) (Figure 6b) show that the Akaba massif rocks are positive anomalies in Ba, Th and negative in Rb, Nb-Ta, P, Zr, Ti. The negative anomalies

in Rb, Nb-Ta and Zr indicate that the magmas in these rocks are linked to a plate convergence magmatic environment (subduction zone). The positive anomaly in Ba suggests that the magmas in these rocks belong to a mantle source. The negative anomaly in Ti reflects the fractionation of ilmenite oxides, while the negative anomaly in P indicates the fractionation of apatite in these rocks.

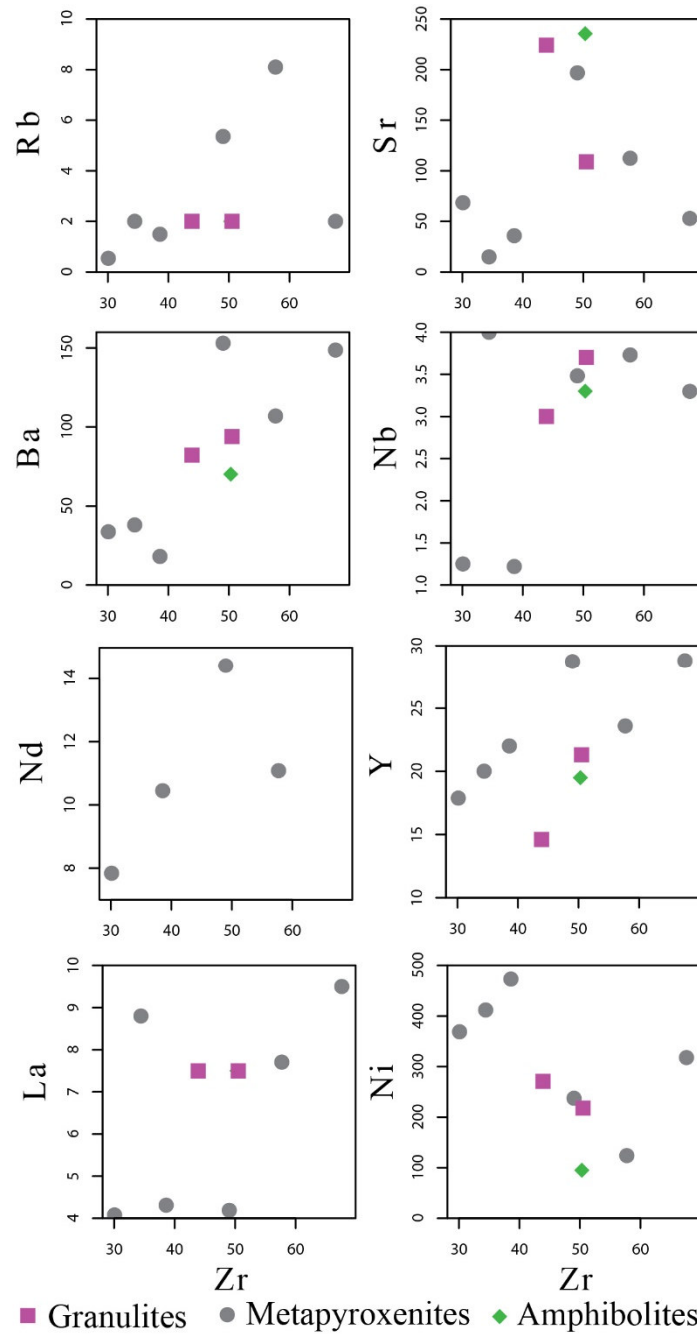


Figure 5. Traces elements (Rb, Sr, Ba, Nb, Nd, Y, La, Ni) versus Zr variation diagrams in Akaba massif rocks (Harker, 1909).

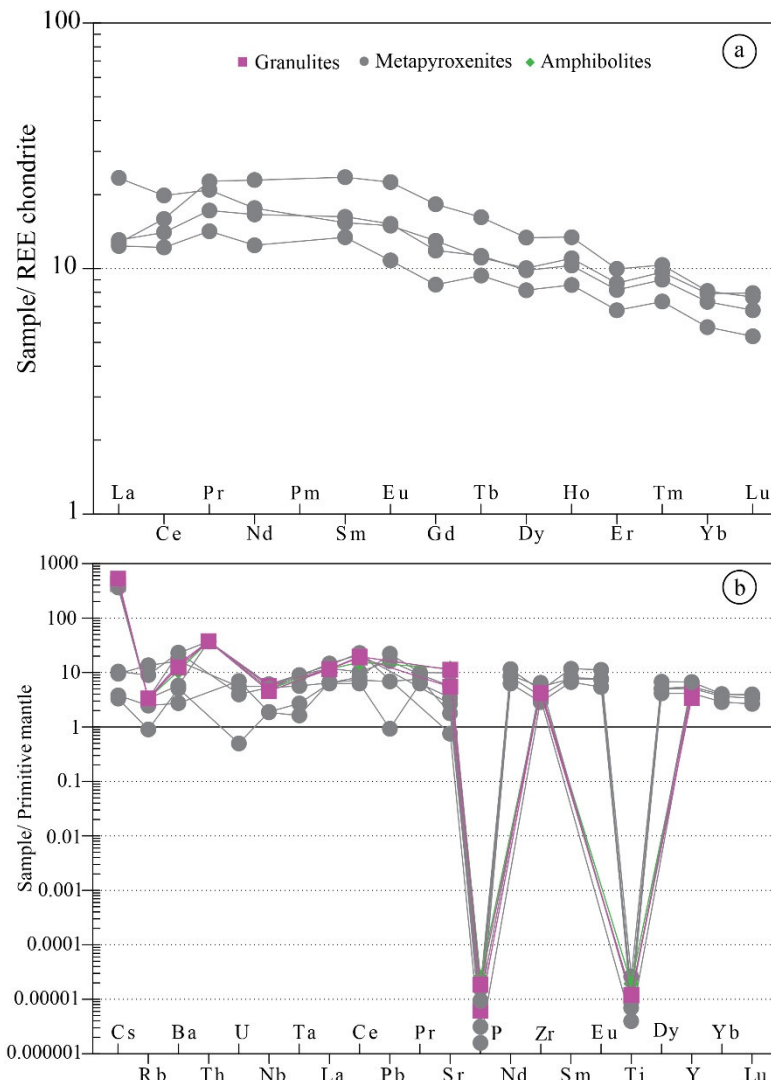


Figure 6. (a) Rare earth elements spectra normalized to chondrites (Nakamura, 1974) and (b) trace elements spectra normalized to the primitive mantle (McDonough & Sun, 1995) of the Akaba massif rocks.

#### 4.2.3 Type of the rocks and geodynamic context

The Akaba massif rocks are distributed in the TAS diagram of Middlemost (1994) (Figure 7a) in the gabbroic diorite and gabbros fields. The diagram of Irvine & Baragar (1971) (Figure 7b) indicates that the rocks in this massif have a tholeiitic affinity. The diagram of Foley *et al.*, (1987) and Shand (1943) (Figure 7c) shows that these rocks are meta- to peraluminous. The diagram of Meschede (1986) (Figure 7d) shows that the rocks of the Akaba massif are N-MORB (D). The one from Pearce & Norry (1979) (Figure 7e) classifies them in the MORB and volcanic arc basalt fields.

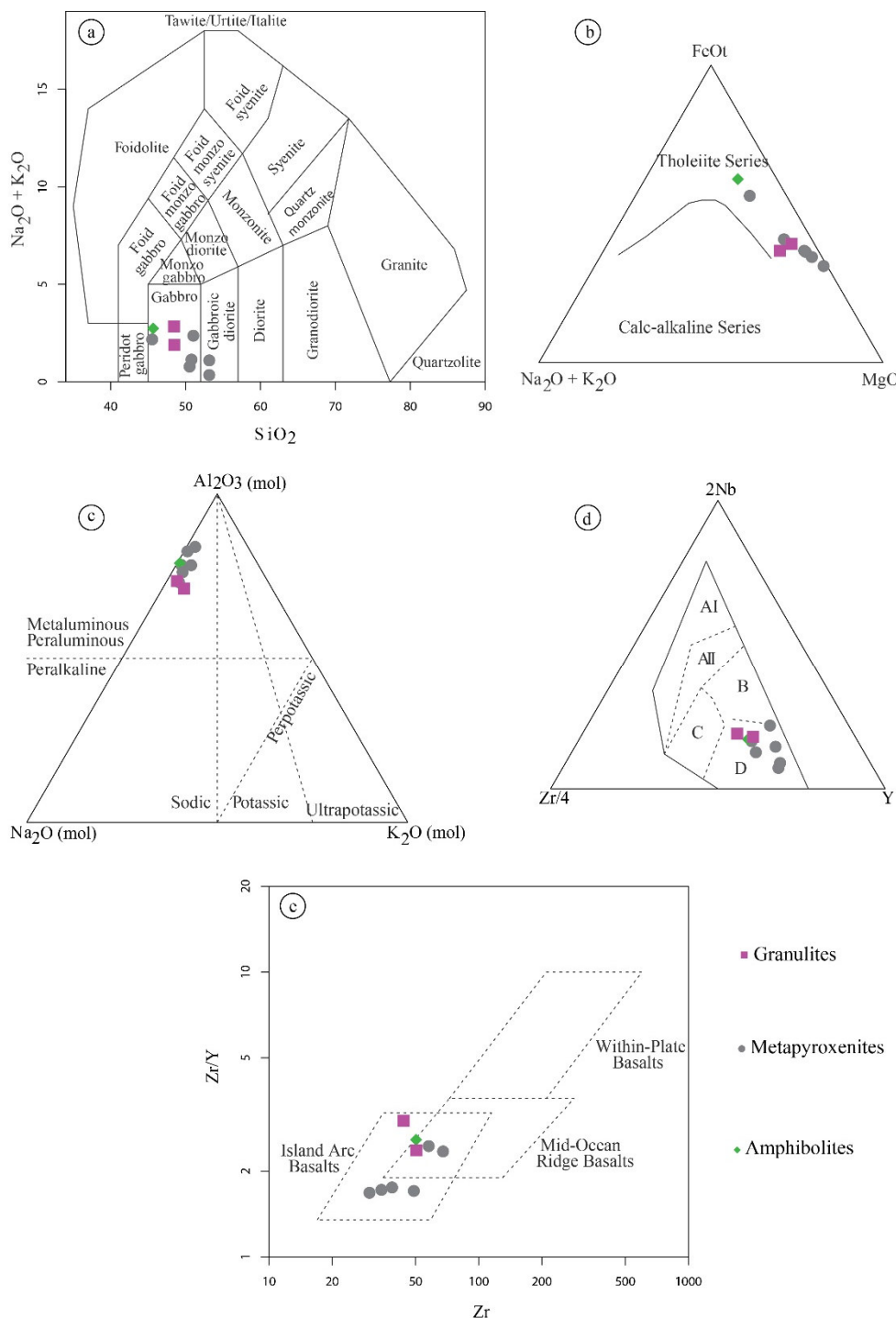


Figure 7. Geochemical classification plots of Akaba massif showing the type (a), magmatic affinities (b and c) and geotectonic context (d and e) of rocks. (a):  $\text{Na}_2\text{O}+\text{K}_2\text{O}$  vs  $\text{SiO}_2$  (Middlemost, 1994); (b):  $\text{FeOt}-(\text{Na}_2\text{O}+\text{K}_2\text{O})-\text{MgO}$  (Irvine & Baragar, 1971); (c):  $\text{Na}_2\text{O}-\text{Al}_2\text{O}_3-\text{K}_2\text{O}$  (mol%) (Foley *et al.*, 1987) and peraluminosity of Shand (1943); (d):  $\text{Zr}/4-\text{Nb}-\text{Y}$  (Meschede, 1986) (AI = intraplate alkaline basalts; AII = intraplate alkaline basalts and tholeiites; B = E-type MORB; C = intraplate tholeiites and volcanic arc basalts; D = N-type MORB); (e):  $\text{Zr}/\text{Y}$  vs  $\text{Zr}$  (Pearce & Norry, 1979).

## 5. Discussion

### 5.1 Petrography and metamorphic evolution

The petrographic study of the Akaba massif shows a diversity of facies: granulites, metapyroxenites and amphibolites. Garnet-free granulites are with a mineralogical assemblage of  $\text{Pl}+\text{Cpx}+\text{Opx}+\text{Hbl}$ . Amphibolitization

has led to the transformation of granulites into amphibolites characterized by Hbl+Pl+Qtz paragenesis, indicating the transition from granulite to amphibolite facies. Metapyroxenites have an Opx+Cpx+Pl+Hbl paragenesis and underwent a first retrograde metamorphism in the amphibolite facies, with the replacement of pyroxenes by green hornblende.

### 5.2 Fractional crystallization

The correlations observed in the Harker variation diagrams for major and trace elements, the parallelism of rare earth elements and multi-element spectra, indicate the evolution of different facies from the unique magmatic source.

The negative anomalies in Nb-Ta and the enrichment in Ba and Th suggest the influence of recycling of crustal material (crustal contamination). The good linear correlation in the Harker diagrams reflects the intervention of a differentiation process by fractional crystallization in the evolution of the parent magmas of the rocks in this massif.

The increase of MgO versus SiO<sub>2</sub> reflects the crystallization of pyroxene, amphibole and ilmenite. The decrease of TiO<sub>2</sub> and P<sub>2</sub>O<sub>5</sub> versus SiO<sub>2</sub> reflects fractional crystallization of ilmenite and apatite. The decrease of Al<sub>2</sub>O<sub>3</sub>, Na<sub>2</sub>O and K<sub>2</sub>O reflects the high alkali feldspar content of these rocks (Guillot *et al.*, 2019; Tairou *et al.*, 2022; Kpanzou, 2023).

The increase of Ba and Th suggests the high fractionation of plagioclase in these rocks. The decrease of Ni versus Zr is compatible with the fractionation of ferromagnesian (pyroxene and amphibole) in these rocks. This element could also be associated with MgO and FeOt in pyroxenes (Hamlaoui *et al.*, 2020; Kpanzou, 2023).

### 5.3 Source of magmas

The Akaba massif rocks have an basic to ultrabasic composition. They have mineralogical and chemical characteristics that allow them to be classified as gabbros and gabbroic diorites according to the terminology of Middlemost (1994). Petrographic characteristics reflect the chemical composition of these rocks with abundant hornblende, the presence of orthopyroxene and clinopyroxene. Negative anomalies of elements such as niobium, phosphorus and titanium, observed on multi-element spectra are fingerprints commonly attributed to subduction zone magmas. The negative anomaly in Nb is characteristic of continental tholeiites and crustal contamination or metasomatism from a mantle source (Guillot *et al.*, 2019; Kpanzou *et al.*, 2022, 2023; Tairou *et al.*, 2022; Kpanzou, 2023).

The genesis of these rocks is therefore compatible with emplacement in a magmatic arc context with simultaneous crustal assimilation and fractional crystallization of magma probably derived from continental crust.

### 5.4 Geotectonic environment

Based on the petrogeochemical data of the Akaba massif rocks, such as their tholeiitic affinity and meta- to peraluminous signature, it can be proposed that they were emplaced in a probably extensive tectonic context (Duclaux, 2003; Guillot *et al.*, 2019; Kpanzou *et al.*, 2022).

Geotectonic discrimination diagrams indicate that these rocks were emplaced in various settings: N-MORB and volcanic arc basalts. The negative anomaly in Nb is characteristic of continental tholeiites and crustal contamination. It suggests a context of subduction zones in which Nb is trapped.

The Akaba massif rocks have similar geochemical characteristics to those of the Kabye, Agou and Djabatoure massifs, such as high Sr and Ba values, a negative anomaly in Nb, and enrichment in light rare earth elements (LREE) compared to heavy rare earth elements (HREE) (Affaton, 1990; Agbossoumondé, 1998; Duclaux, 2003; Sabi, 2007; Kpanzou, 2023) and subsequently contaminated by continental crust (Agbossoumondé *et al.*, 2017; Liégeois, 2019; Aidoo *et al.*, 2020; Kpanzou, 2023; Kpanzou *et al.*, 2023).

Despite the lack of isotopic data, petrogeochemical studies of the Akaba massif rocks show similarities with those of the Kabye, Agou and Djabatoure massifs, allowing them to be classified in the same geodynamic context.

## 6. Conclusion

Petrographic studies of the Akaba massif have identified: granulites, metapyroxenites and amphibolites. The mineralogies of these rocks are dominated by a primary paragenesis constituted by an abundance of plagioclase followed by clinopyroxene, and a secondary paragenesis which is mainly represented by alteration minerals such as amphibole and iron and titanium oxides. These paragenesis show that these rocks underwent metamorphism in the granulite facies with retrogression in the amphibolite facies. Thus, the massif has undergone a metamorphic evolution from granulitization to retrograde metamorphism in amphibolite facies.

Geochemical characterization shows that the rocks of the Akaba massif display meta- to peraluminous and tholeiitic affinity. Inter-element variations indicate that these rocks evolved from a fractional crystallization process accompanied by crustal contamination. They were emplaced in various settings: N-MORB and volcanic arc basalts. They are crustal base rocks uplifted by Pan-African tectonics in crustal sets. Geochemical trends clearly indicate their emplacement in a subduction context.

The Akaba massif rocks show enrichment in LREE compared to HREE, and sub-flat HREE spectra. Multi-element spectra show that most of the rocks are rich in mobile elements (Ba and Th) and have negative anomalies in Nb-Ta, P and Ti. These characteristics are similar to those of rocks from a mantle source enriched and metasomatized during a subduction event.

#### Acknowledgement

I would like to thank the authorities of the universities of the Coimbra Group who, through the "Coimbra Group Short Stay Scholarship Programme for young researchers from Sub-Saharan Africa", have granted me a laboratory research scholarship for the realization of geochemical analyses of rock samples. I also thank Professors Antonio Garcia-Casco and José María González-Jiménez, both professors-researchers at the Department of Petrology and Mineralogy of the University of Granada in Spain, who agreed to support my application for the scholarship and to carry out the chemical analyses of my rock samples in their laboratory. We acknowledge the anonymous reviewers for their constructive comments which improve the quality of the initial manuscript.

#### References

- Affaton, P. (1990). Le bassin des Volta (Afrique de l'Ouest) : une marge passive d'âge protérozoïque supérieur, tectonisée au Panafricain (600±50 Ma). Edit. ORSTOM, Collection Etudes & Thèses, Paris, 500p. [https://horizon.documentation.ird.fr/exl-doc/pleins\\_textes/pleins\\_textes\\_2/etudes\\_theses/31718.pdf](https://horizon.documentation.ird.fr/exl-doc/pleins_textes/pleins_textes_2/etudes_theses/31718.pdf).
- Affaton, P., Gelard, J.P. & Simpara, N. (1991). Paléocontraintes enregistrées par la fracturation dans l'unité structurale de l'Atacora (Chaîne Panafricaine des Dahomeyides, Togo). C. R. Acad. Sci., Paris, t. 312 : 763-768. <http://pascal-francis.inist.fr/vibad/index.php?action=getRecordDetail&idt=19679359>.
- Agbossoumondé, Y. (1998). Les complexes ultrabasiques de la chaîne panafricaine au Togo (Axe Agou – Atakpamé, Sud-Togo). Etude pétrographique, minéralogique et géochimique. Thèse Doct. Lab. Géol. Pétro. Univ. Jean Monnet St. Etienne Fr., 306p.
- Agbossoumondé, Y., Ménot, R.-P. & Guillot, S. (2001). Metamorphic evolution of Neoproterozoic eclogites from South Togo (West Africa). Jour. of Afr. Earth Sc. [https://doi.org/10.1016/S0899-5362\(01\)80061-0](https://doi.org/10.1016/S0899-5362(01)80061-0) 33, 227–244.
- Agbossoumondé, Y., Ménot, R.-P., Paquette, J.L., Guillot, S., Yéssoufou, S. & Perrache, C. (2007). Petrological and geochronological constraints on the origin of the Palimé–Amlamé granitoids (South Togo, West Africa): A segment of the West African Craton Paleoproterozoic margin reactivated during the Pan-African collision. Gondwana Research 12, 476–488. <https://doi.org/10.1016/j.gr.2007.01.004>
- Agbossoumondé, Y., Ménot, R.-P. & Ganade de Araujo, C.E. (2017). Major, Trace Elements and Sr-Nd Isotopic Characteristics of High-Pressure and Associated Metabasites from the Pan-African Suture Zone of Southern Togo, West Africa, 15p.
- Aidoo, F., Sub, F.-Y., Liang, T. & Nude, P.M. (2020). New insight into the Dahomeyide Belt of southeastern Ghana, West Africa: Evidence of arc-continental collision and Neoarchaean crustal reworking. Precambrian Research 347 (2020) 105836. <https://doi.org/10.1016/j.precamres.2020.105836>.
- Alayi, G. (2018). Les granitoïdes tardifs de la chaîne panafricaine des Dahomeyides au Togo : étude pétro-structurale, géochimique et géochronologique. Thèse de Doctorat, FDS, Univ. Lomé-Togo, 256p.
- Attoh, K. (1998). High-Pressure Granulite Facies metamorphism in the Pan-African Dahomeyide orogen, West Africa. J. Geology, 106 : 236-246. <https://doi.org/10.1086/516019>
- Attoh, K., Dallmeyer, R.D. & Affaton, P. (1997). Chronology of nappe assembly in the Pan-Africa Dahomeyide Orogen, West Africa : evidence from 40Ar/39Ar mineral ages. Precambrian research, 82, pp. 153 – 171. [https://doi.org/10.1016/S0301-9268\(96\)00031-9](https://doi.org/10.1016/S0301-9268(96)00031-9)
- Attoh, K. & Morgan, J. (2004). Geochemistry of high-pressure granulites from the Pan-African Dahomeyide orogen, West Africa: constraints on the origin and composition of lower crust. Jour.of Afr.Earth Sci., vol. 39, pp. 201-208. <https://doi.org/10.1016/j.jafrearsci.2004.07.048>
- Caby, R., Bertrand, J.M. & Black, R. (1981). Pan-African closure and continental collision in the Hoggar. Ifora segment, central Sahara. In Kröner A. (Eds) Precambrian Plate Tectonics. Elsevier, Amst, pp. 407-434.
- Caby, R. & Boessé, J.M. (2001). Pan-African nappe system in southwest Nigeria : the Ife– Ilesha schist belt. Jour.of Afr.Earth Sci., vol. 33 n°2, pp.211-225. DOI: 10.1016/S0899-5362(01)80060-9.
- Duclaux, G. (2003). Etude pétrologique et structurale des massifs basiques et ultrabasiques de la zone de suture panafricaine de la chaîne des Dahomeyides au Togo : Implications géodynamiques. Mém. DEA, Lab. Dyn. Lithos. Univ. J. Monnet, St-Etienne, 29p. <https://doi.org/DOI:10.13140/RG.2.2.28332.92809>
- Ganade de Araujo, C.E., Rubatto, D., Hermann, J., Cordani, U.G., Caby, R. & Basei, M.A.S. (2014a). Ediacaran 2,500-km-long synchronous deep continental subduction in the West Gondwana Orogen. Nature Communications, 5:5198. doi: 10.1038/ncomms6198.
- Guillot, S., Agbossoumondé, Y., Bascou, J., Berger, J., Duclaux, G., Hilairet, N., Ménot, R.-P. & Schwartz, S. (2019). Transition from subduction to collision recorded in the Pan-African arc complexes (Mali to Ghana).

- Precambrian Research 320 (2019): 261–280.
- Hamlaoui, H., Laouar, R., Bouhle, S. & Boyce, A.J. (2020). Caractéristiques pétrologiques et géochimiques des roches magmatiques d'El Aouana, NE algérien". Estudios Geológicos enero-junio, e124 ISSN-L: 0367-0449, 76(1). <https://doi.org/10.3989/egeol.43391.510>.
- Harker, A. (1909). The natural history of igneous Rocks. Methuen and Co., London, 384p. <https://doi.org/10.1017/CBO9780511920424>
- Irvine, T.N. & Baragar, W.R.A. (1971). A guide to chemical classification of the common volcanic rocks. Can. J. Earth Sci., 8 : 523-548. <https://doi.org/10.1139/e71-055>
- Kpanzou, S.A.M. (2017). Etude pétrographique et structurale du massif de Djabatouré et des massifs adjacents. Mém. Master, FDS, Univ. Lomé, 31p.
- Kpanzou, S.A.M. (2023). Contribution à l'étude du complexe basique-ultrabasique de Djabatouré-Anié (Centre-Togo) : Caractéristiques pétrostructurales, géochimiques et indices de minéralisations associés. Thèse de Doctorat unique, FDS, Univ. Lomé, 232p.
- Kpanzou, S.A.M., Agbossoumondé, Y. & Tairou, M.S. (2019). Caractérisation pétrostructurale du massif granulitique de Djabatouré. J. Rech. Sci. Univ. Lomé (Togo), Spécial 2019, 21(4-2) : 509-519. <https://www.ajol.info/index.php/jrsul/article/view/206992>.
- Kpanzou, S.A.M., Agbossoumondé, Y., González Jiménez, J.M., Tairou, M.S. & Garcia-Casco, A. (2022). Pétrologie et métallogénie des indices de Ni-Cr associés au massif basique-ultrabasique de Oké, Togo. Afrique SCIENCE 21(1) : 53 - 69. <https://www.afriquescience.net/PDF/21/1/5.pdf>.
- Kpanzou, S.A.M., Alayi, G., Agbossoumondé, Y., Tairou, M.S., González Jiménez, J.M. & Garcia-Casco, A. (2023). Petrographic and Geochemical Characteristics of the Djabatoure Massif Metamigmatites from the Pan-African Orogen in Central Togo, West Africa. European Scientific Journal, ESJ, 19 (24), 198. <https://doi.org/10.19044/esj.2023.v19n24p198>.
- Kwayisi, D., Elburg, M. & Lehmann, J. (2021). Preserved ancient oceanic lithosphere within the Buem structural unit at the eastern margin of the West African craton, LITHOS (2021), <https://doi.org/10.1016/j.lithos.2021.106585>.
- Liégeois, J.P. (2019). New synthetic Geological Map of the Tuareg shield: An Overview of its Global structure and Geological Evolution. Springer, Geology Switzerland, 83p. [https://apps.umc.edu.dz/vrp/virtualseminar/doc/Proceeding\\_Magmatism\\_Precambrian\\_bases\\_petrography.pdf](https://apps.umc.edu.dz/vrp/virtualseminar/doc/Proceeding_Magmatism_Precambrian_bases_petrography.pdf).
- McDonough, W.F. & Sun, S.S. (1995). The composition of the Earth. Chemical Geology 120, pp. 223–253. [https://doi.org/10.1016/0009-2541\(94\)00140-4](https://doi.org/10.1016/0009-2541(94)00140-4)
- Ménot, R.-P. (1977). Les massifs basiques et ultrabasiques antémétamorphiques de la bordure Ouest du mole Dahoméo-nigérian. Essai de synthèse bibliographique. Ann. Univ. Bénin, Lomé, pp. 53–94.
- Ménot, R.-P. (1980). Les massifs basiques et ultrabasiques de la zone mobile panafricaine au Ghana, Togo et au Bénin. Etat de la question. Bull. soc. Géol. Fr., 7 : 297–303. <https://doi.org/DOI:10.2113/gssgbull.S7-XXII.3.297>
- Ménot, R.-P. (1982). Les éclogites des Monts Lato : un témoin de l'évolution tectono-métamorphique de la chaîne pan-africaine du Togo (Afrique de l'Ouest). Ist. intern. Eclogite Conf., Terra Cognita, 2, (3), 320p.
- Ménot, R.-P. & Seddoh, K.F. (1980). Le massif basique stratifié précambrien de Djabatoure-Soutouboua (région centrale du Togo, Afrique de l'Ouest). Pétrologie et évolution métamorphique. Bulletin du B.R.G.M. 4(4) : 319–337.
- Ménot, R.-P. & Seddoh, K.F. (1985). The eclogites of Lato Hills (South Togo, West Africa) : relies from early tectonometamorphic evolution of the Pan-African orogeny. Chemical Geology, 50, pp. 313–330. [https://doi.org/10.1016/0009-2541\(85\)90126-3](https://doi.org/10.1016/0009-2541(85)90126-3)
- Meschede, M. (1986). A method of discrimination between different types of mid-ocean ridge basalts and continental tholeiites with Nb-Zr-Y diagram. Chemical Geology, 56 : 207-218. [https://doi.org/10.1016/0009-2541\(86\)90004-5](https://doi.org/10.1016/0009-2541(86)90004-5)
- Middlemost, E.A.K. (1994). Naming materials in the magma/igneous rock system. Earth Science Reviews, 37 (3-4), pp. 215-224.
- Nakamura, N. (1974). Determination of REE, Fe, Mg, Na and K in Carbonaceous and ordinary Chondrites. Geochemica et Cosmochimica Acta, 38, 757-775. [http://dx.doi.org/10.1016/0016-7037\(74\)90149-5](http://dx.doi.org/10.1016/0016-7037(74)90149-5)
- Pearce, J.A. & Norry, M.J. (1979). Petrogenetic implications of Ti, Zr, Y and Nb variations in volcanics rocks. Contrib. Mineral. Petrol., 69 : 33-92.
- Sabi, B.E. (2007). Etude pétrologique et structurale du Massif Kabyè, Nord-Togo. Thèse Doctorat, FDS, Univ. Lomé, 256p.
- Shand, S.J. (1943). Eruptive Rocks. Their Genesis, Composition, Classification and Their Relations to Ore deposits. 2nd edition, Murby London, 444p.
- Sylvain, J.P., Collart, J., Aregba, A. & Godonou, S. (1986). Notice explicative de la carte géologique 1/500.0000 è

- du Togo, Mém. n°6, D.G.M.G. / B.N.R.M., Lomé – Togo.
- Tairou, M.S., Affaton, P., Sabi, B.E. & Seddoh, K.F. (2009). Tectono-metamorphic evolution of the Mo and Kara-Niamtougou Orthogneic Suites, Northern Togo. Global Jour. of Geological Sciences, vol. 7, n°2, pp. 93-100.
- Tairou, M.S. & Affaton, P. (2013). Structural Organization and Tectono-Metamorphic Evolution of the Pan-African Suture Zone: Case of the Kabye and Kpaza Massifs in the Dahomeyide Orogen in Northern Togo (West Africa). International Journal of Geosciences 04, 166–182. <https://doi.org/10.4236/ijg.2013.41015>
- Tairou, M.S., Miningou, Y.M.W., Da Costa, Y.D. & Kwekam, M. (2022). Petrostructural and Geochemical Characteristics of the Metamagmatites in the External Zone of the Dahomeyides Belt: Case of the Kantè Serpentinites (Northern Togo). International Journal of Geosciences, 2022, 13, 779-792. <https://www.scirp.org/journal/ijg>.